

# Constraints on the axial-vector and pseudo-scalar mediated WIMP-nucleus interactions from PandaX-4T experiment

Zhou Huang,<sup>1</sup> Chencheng Han,<sup>2</sup> Abdusalam Abdukerim,<sup>1</sup> Zihao Bo,<sup>1</sup> Wei Chen,<sup>1</sup> Xun Chen,<sup>1,3</sup> Yunhua Chen,<sup>4</sup> Chen Cheng,<sup>5</sup> Zhaokan Cheng,<sup>6</sup> Xiangyi Cui,<sup>2</sup> Yingjie Fan,<sup>7</sup> Deqing Fang,<sup>8</sup> Changbo Fu,<sup>8</sup> Mengting Fu,<sup>9</sup> Lisheng Geng,<sup>10,11,12</sup> Karl Giboni,<sup>1</sup> Linhui Gu,<sup>1</sup> Xuyuan Guo,<sup>4</sup> Ke Han,<sup>1</sup> Changda He,<sup>1</sup> Jinrong He,<sup>4</sup> Di Huang,<sup>1</sup> Yanlin Huang,<sup>13</sup> Ruquan Hou,<sup>3</sup> Xiangdong Ji,<sup>14</sup> Yonglin Ju,<sup>15</sup> Chenxiang Li,<sup>1</sup> Jiafu Li,<sup>5</sup> Mingchuan Li,<sup>4</sup> Shu Li,<sup>15</sup> Shuaijie Li,<sup>2</sup> Qing Lin,<sup>16,17</sup> Jianglai Liu,<sup>1,2,3,\*</sup> Xiaoying Lu,<sup>18,19</sup> Lingyin Luo,<sup>9</sup> Yunyang Luo,<sup>17</sup> Wenbo Ma,<sup>1</sup> Yugang Ma,<sup>8</sup> Yajun Mao,<sup>9</sup> Nasir Shaheed,<sup>18,19</sup> Yue Meng,<sup>1,3</sup> Xuyang Ning,<sup>1</sup> Ningchun Qi,<sup>4</sup> Zhicheng Qian,<sup>1</sup> Xiangxiang Ren,<sup>18,19</sup> Changsong Shang,<sup>4</sup> Xiaofeng Shang,<sup>1</sup> Guofang Shen,<sup>10</sup> Lin Si,<sup>1</sup> Wenliang Sun,<sup>4</sup> Andi Tan,<sup>14</sup> Yi Tao,<sup>1,3</sup> Anqing Wang,<sup>18,19</sup> Meng Wang,<sup>18,19</sup> QiuHong Wang,<sup>8</sup> Shaobo Wang,<sup>1,20</sup> Siguang Wang,<sup>9</sup> Wei Wang,<sup>6,5</sup> Xiuli Wang,<sup>15</sup> Zhou Wang,<sup>1,3,2</sup> Yuehuan Wei,<sup>6</sup> Mengmeng Wu,<sup>5</sup> Weihao Wu,<sup>1</sup> Jingkai Xia,<sup>1</sup> Mengjiao Xiao,<sup>14</sup> Xiang Xiao,<sup>5</sup> Pengwei Xie,<sup>2</sup> Binbin Yan,<sup>1</sup> Xiyu Yan,<sup>13</sup> Jijun Yang,<sup>1</sup> Yong Yang,<sup>1</sup> Chunxu Yu,<sup>7</sup> Jumin Yuan,<sup>18,19</sup> Ying Yuan,<sup>1</sup> Zhe Yuan,<sup>8</sup> Xinning Zeng,<sup>1</sup> Dan Zhang,<sup>14</sup> Minzhen Zhang,<sup>1</sup> Peng Zhang,<sup>4</sup> Shibo Zhang,<sup>1</sup> Shu Zhang,<sup>5</sup> Tao Zhang,<sup>1</sup> Yingxin Zhang,<sup>18,19</sup> Yuanyuan Zhang,<sup>2</sup> Li Zhao,<sup>1</sup> Qibin Zheng,<sup>13</sup> Jifang Zhou,<sup>4</sup> Ning Zhou,<sup>1,†</sup> Xiaopeng Zhou,<sup>10</sup> Yong Zhou,<sup>4</sup> and Yubo Zhou<sup>1</sup>  
(PandaX Collaboration)

<sup>1</sup>*School of Physics and Astronomy, Shanghai Jiao Tong University, Key Laboratory for Particle Astrophysics and Cosmology (MoE), Shanghai Key Laboratory for Particle Physics and Cosmology, Shanghai 200240, China*

<sup>2</sup>*Tsung-Dao Lee Institute, Shanghai Jiao Tong University, Shanghai, 200240, China*

<sup>3</sup>*Shanghai Jiao Tong University Sichuan Research Institute, Chengdu 610213, China*

<sup>4</sup>*Yalong River Hydropower Development Company, Ltd., 288 Shuanglin Road, Chengdu 610051, China*

<sup>5</sup>*School of Physics, Sun Yat-Sen University, Guangzhou 510275, China*

<sup>6</sup>*Sino-French Institute of Nuclear Engineering and Technology, Sun Yat-Sen University, Zhuhai, 519082, China*

<sup>7</sup>*School of Physics, Nankai University, Tianjin 300071, China*

<sup>8</sup>*Key Laboratory of Nuclear Physics and Ion-beam Application (MOE), Institute of Modern Physics, Fudan University, Shanghai 200433, China*

<sup>9</sup>*School of Physics, Peking University, Beijing 100871, China*

<sup>10</sup>*School of Physics, Beihang University, Beijing 102206, China*

<sup>11</sup>*International Research Center for Nuclei and Particles in the Cosmos & Beijing Key Laboratory of Advanced Nuclear Materials and Physics, Beihang University, Beijing 100191, China*

<sup>12</sup>*School of Physics and Microelectronics, Zhengzhou University, Zhengzhou, Henan 450001, China*

<sup>13</sup>*School of Medical Instrument and Food Engineering, University of Shanghai for Science and Technology, Shanghai 200093, China*

<sup>14</sup>*Department of Physics, University of Maryland, College Park, Maryland 20742, USA*

<sup>15</sup>*School of Mechanical Engineering, Shanghai Jiao Tong University, Shanghai 200240, China*

<sup>16</sup>*State Key Laboratory of Particle Detection and Electronics, University of Science and Technology of China, Hefei 230026, China*

<sup>17</sup>*Department of Modern Physics, University of Science and Technology of China, Hefei 230026, China*

<sup>18</sup>*Research Center for Particle Science and Technology, Institute of Frontier and Interdisciplinary Scienc, Shandong University, Qingdao 266237, Shandong, China*

<sup>19</sup>*Key Laboratory of Particle Physics and Particle Irradiation of Ministry of Education, Shandong University, Qingdao 266237, Shandong, China*

<sup>20</sup>*SJTU Paris Elite Institute of Technology, Shanghai Jiao Tong University, Shanghai, 200240, China*

(Dated: August 9, 2022)

We present the constraints on the axial-vector and pseudo-scalar mediated WIMP-nucleus interactions from the PandaX-4T experiment, using the data set corresponding to a total exposure of 0.63 tonne-year. No significant signal excess is observed, and the most stringent upper limits to date on the spin-dependent WIMP-neutron scattering cross section are set at 90% confidence level with the minimum WIMP-neutron scattering cross section of  $5.8 \times 10^{-42} \text{cm}^2$  for WIMP mass of 40 GeV/ $c^2$ . Exclusion limits on the axial-vector and pseudo-scalar simplified models are also derived.

There are plenty of evidences indicating that a large amount of dark matter exists in our universe. However its nature is still elusive [1]. Weakly interacting massive particle (WIMP) is a plausible dark matter candi-

date which arises from super-symmetry model naturally. Various methods are utilized to hunt for WIMPs, including direct search, indirect search and the collider search. Based on the dual-phase xenon time projection chamber

(TPC), the sensitivity of WIMP-nucleus interaction has been improved significantly over the past decades [2–7].

The PandaX-4T experiment, located at the China Jinping Underground Laboratory (CJPL) [8, 9], is one of the largest xenon TPC experiments with 3.7-tonne of liquid xenon in the sensitive volume. The cylindrical TPC is covered by 24 polytetrafluoroethylene (PTFE) panels on the side and 368 Hamamatsu R11410-23 3-inch photomultiplier tubes (PMTs) on the top and bottom, with four electrodes placed inside to construct the drift and extraction electric field. Once an incoming energetic particle scatters off xenon nuclei or electron, prompt scintillation light ( $S1$ ) and ionized electrons are generated, the latter then drift upward to the liquid xenon surface and produce the electroluminescence light ( $S2$ ) in the gaseous xenon region under the electric fields. Both  $S1$  and  $S2$  are detected by the PMTs, from which the scattering position and deposited energy can be reconstructed. The ratio of  $S2$  to  $S1$  provides a powerful signal-background discrimination. More detailed description of PandaX-4T experiment can be found in Refs. [5, 10, 11].

The PandaX-4T experiment has set stringent constraints on the spin-independent (SI) WIMP-nucleon cross section upper limits, excluding  $3.8 \times 10^{-47} \text{cm}^2$  at  $40 \text{ GeV}/c^2$  WIMP mass and 90% confidence level (C.L.) [5]. The SI WIMP-nucleus interaction can be introduced by vector or scalar mediators with couplings to WIMPs and quarks in the simplified models. For axial-vector and pseudo-scalar mediators, the tree-level processes yield spin-dependent (SD) WIMP-nucleus interactions instead [12, 13]. Xenon-based experiments are also sensitive to the SD interactions thanks to the significant abundance of odd- $A$  xenon isotopes with non-zero spin (26.4% spin-1/2  $^{129}\text{Xe}$  and 21.2% spin-3/2  $^{131}\text{Xe}$  in natural xenon) [14, 15]. The XENON1T experiment has pushed down the SD neutron-only cross-section limits to  $6.3 \times 10^{-42} \text{cm}^2$  at  $30 \text{ GeV}/c^2$  WIMP mass and 90% C.L.. In this letter, we present the search results of SD WIMP-nucleus interactions and constraints on the corresponding mediators, based on the PandaX-4T commissioning run data. For pseudo-scalar mediator, due to the momentum suppression on the tree-level SD process, constraints are derived from the loop-level SI process instead.

As for axial-vector couplings to quarks and WIMPs, the WIMP-nucleus SD cross section can be evaluated from chiral effective field theory (EFT) [16–18], which is related to the total spin expectation values of the protons and neutrons in the nucleus in the limit of zero momentum transfer. Therefore, a common practice is to consider two special cases where the WIMPs couple only to protons or to neutrons. The corresponding scattering cross section is expressed as below,

$$\sigma_A = \frac{4\pi}{3(2J+1)} \left( \frac{\mu_A}{\mu_N} \right)^2 S_N(q^2) \sigma_N, \quad (1)$$

where  $N$  denotes the proton ( $p$ ) or neutron ( $n$ ),  $\mu_N$  is the

reduced mass for WIMP scattering off the nucleon,  $\mu_A$  is the reduced mass of WIMP and the target nucleus,  $S_N(q^2)$  is the structure factor for “proton-only” or “neutron-only” cases [16]. Due to the cancellation between spins of nucleon pairs, the SD cross section with nucleus is dominated by the unpaired nucleon, which is neutron for  $^{129}\text{Xe}$  and  $^{131}\text{Xe}$ . It should be noticed that the cross section of “proton-only” case is significantly enhanced due to chiral two-body currents involving the exchange of a pion.

The differential event rate for the WIMP SD interaction can be then written as [19, 20]

$$\frac{dR}{dE} = \frac{\rho_\chi \sigma_A}{2m_\chi \mu_A^2} \eta(E), \quad (2)$$

where  $m_\chi$  and  $\rho_\chi$  are the WIMP mass and local density respectively,  $\sigma_A$  is the WIMP-nucleus cross section,  $\eta$  is the mean inverse speed of WIMP velocity distribution. It is recommended that  $\rho_\chi = 0.3 \text{ GeV}/(c^2 \cdot \text{cm}^3)$  and the WIMP motion obeys the standard halo model [21]. Explicitly, the most probable velocity of WIMP in Maxwellian distribution  $v_0 = 238 \text{ km/s}$ , the galactic escape velocity  $v_{\text{esc}} = 544 \text{ km/s}$  and the Earth velocity  $v_E = 254 \text{ km/s}$  are adopted in this analysis. The typical event rate as a function for nuclear recoil energy is shown in Fig. 1. Both the SD “proton-only” and “neutron-only” recoil energy spectra are plotted in addition to the SI case for the WIMP mass of  $40 \text{ GeV}/c^2$  and  $400 \text{ GeV}/c^2$ , with the detection efficiency [5] overlaid.

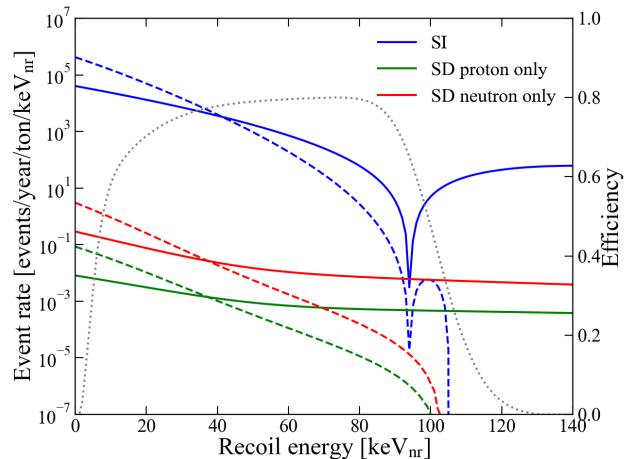


FIG. 1. Nuclear recoil energy spectra for the scattering of WIMP on PandaX-4T detector. The SI, SD proton-only, SD neutron-only are illustrated in blue, green and red curves with  $\sigma = 10^{-41} \text{cm}^2$  respectively. The dashed and solid curves represent the  $40 \text{ GeV}/c^2$  and  $400 \text{ GeV}/c^2$  WIMPs respectively. The detection efficiency of PandaX-4T experiment is plotted in dotted curve with the corresponding axis on the right.

We use the same data set and selections as the WIMP SI analysis [5]. In brief, the  $S1$  signal region of interest requires the  $S1$  in the range of 2 to 135 photoelectron(PE)

in the fiducial volume, and the  $S2$  signal collected in the bottom PMT array ( $S2_b$ ) is adopted to avoid bias from PMT saturation. The data is divided into five subsets, according to the detector status. The background models also inherit from Ref. [5] and the detailed values can be found in the Table II of Ref. [5]. The total live time is 86.0 days and the resulting exposure is 0.63 tonne-year.

The 90% confidence level (C.L.) upper limit of SD WIMP-nucleon cross section as a function of WIMP mass is calculated, utilizing the same statistical inference (profile likelihood ratio) in Ref. [5, 21]. The results are shown in Fig. 2 and Fig. 3, for “neutron-only” and “proton-only” interaction respectively. Selected experiment results are also plotted for comparison. In the WIMP mass above  $6 \text{ GeV}/c^2$  region, the most stringent upper limit for “neutron-only” interaction in direct detection experiment is obtained, with a minimal cross section (90% C.L.) of  $5.8 \times 10^{-42} \text{ cm}^2$  at  $40 \text{ GeV}/c^2$  and C.L. is obtained. For the “proton-only” interaction, the xenon detector technique is not competitive to PICO-60 [22] and the minimal cross section of  $1.7 \times 10^{-40} \text{ cm}^2$  for  $40 \text{ GeV}/c^2$  WIMP is obtained.

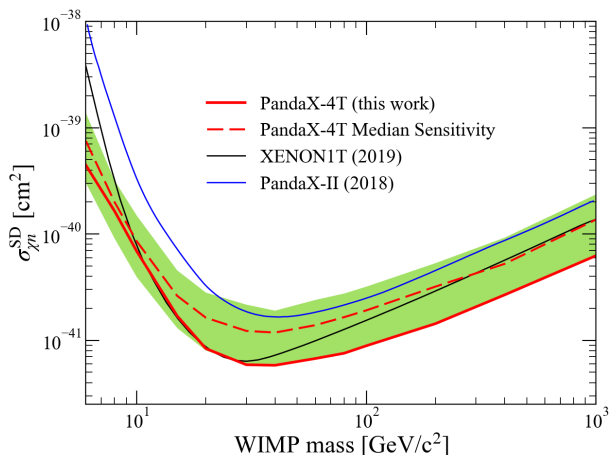


FIG. 2. PandaX-4T 90% C.L. upper limit for the SD WIMP-neutron cross section, overlaid with that from XENON1T 2019 [15] and PandaX-II 2018 [14]. The green band and dashed red curve represent the  $\pm 1\sigma$  sensitivity band and the median, respectively.

Constraints on the WIMP parameter space can be also provided by collider experiments such as the ATLAS under various model assumptions. The benchmark models with mediators at the LHC are summarized in Refs. [23–25]. We consider two simplified models with an axial-vector mediator and a pseudo-scalar mediator respectively in this letter.

When the mediator is axial-vector, the mediator couples to all quark flavors equally with one unique coupling constant  $g_q$ , and thus it yields isoscalar couplings to neutrons and protons. In this model, there are four free parameters: WIMP mass  $m_\chi$ , mediator mass  $m_V$ , the

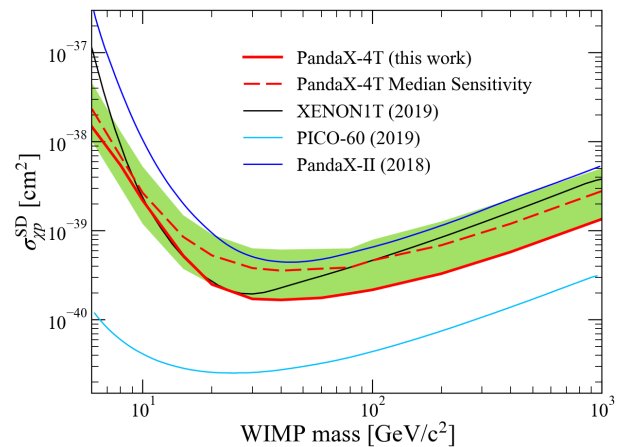


FIG. 3. PandaX-4T 90% C.L. upper limit for the SD WIMP-proton cross section, overlaid with that from XENON1T 2019 [15], PandaX-II 2018 [14] and PICO-60 2019 [22]. The green band and dashed red curve represent the  $\pm 1\sigma$  sensitivity band and the median, respectively.

coupling of the mediator to WIMP  $g_\chi$  and the coupling of the mediator to quark  $g_q$ . Following the Ref. [26], both the tree-level amplitudes and the loop-level amplitudes are calculated, and the latter is negligible. The cross section is given in Ref. [24, 26] with the form

$$\sigma_{\chi N}^{\text{SD}} = \frac{0.31 g_q^2 g_\chi^2 \mu_N^2}{\pi m_V^4}, \quad (3)$$

where couplings  $g_q = 0.25$  and  $g_\chi = 1$  are adopted as a benchmark scenario. Based on this model, the signal energy spectra are generated and the same analysis method is applied. The 95% C.L. exclusion limit on mediator mass is obtained as shown in Fig. 4, with comparisons to collider experiments [27, 28], and other direct detection experiments [15, 29]. In addition, the renormalization group evolution (RGE) effect is considered to account for the corrections from mediator mass scale to the nuclear scale in direct detection [30]. The limit on the mediator mass with RGE effect is also shown in Fig. 4.

In the scenario of pseudo-scalar mediator model, which contains the SD tree-level contribution. However, the amplitudes are momentum-suppressed [31, 32]. The only non-suppressed amplitudes are from the SI interactions induced by loop diagrams. A distinct model, referred as 2HDM+a model, is recommended by the ATLAS/CMS DM Forum [23]. It is one of the simplest gauge-invariant and renormalizable extension of the simplified pseudo-scalar model. It contains Higgs doublets ( $h/H$ ) and a pseudo-scalar mediator ( $a$ ). Following Ref. [12, 32, 33], the loop-level amplitudes are calculated from the effective Lagrangian. The loop level diagrams are shown as Fig. 5. The cross section is given by

$$\sigma_{\chi N}^{\text{SI}} = \frac{\mu_N^2 |C_N^{\text{loop}}|^2}{\pi}, \quad (4)$$

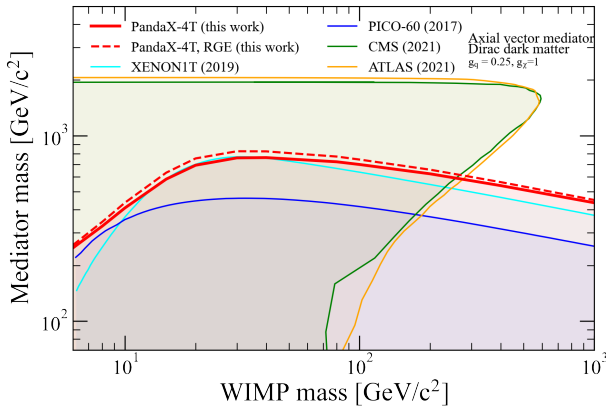


FIG. 4. PandaX-4T 95% C.L. exclusion limit on the mediator mass for a simplified isoscalar model with an axial-vector mediator and a Dirac WIMP, where the coupling constants  $g_q$  and  $g_\chi$  are 0.25 and 1, respectively. RGE effect is considered in the limit shown as dashed red line. The results from other direct detection experiments, XENON1T [15] and PICO-60 [29], and collider experiments, ATLAS [27] and CMS [28], are shown for comparison.

where the coefficient  $C_N^{\text{loop}}$  includes 11 free parameters, as described in Ref. [23]. In this letter, the following conventional values are adopted:

$$\begin{aligned} \tan(\beta) &= 10, \alpha = \beta + \frac{\pi}{2}, m_h = 125 \text{ GeV}, \\ m_H &= m_{H^\pm} = m_A = 600 \text{ GeV}, m_a = 250 \text{ GeV}, \\ \theta &= 0.1, c_1 = 0, c_2 = 1, g_\chi = 1, \end{aligned} \quad (5)$$

where  $\alpha$ ,  $\beta$  and  $\theta$  are the rotation angles.  $c_1$  and  $c_2$  are the coefficients of the quartic term in the interaction.  $g_\chi$  is the coupling constant between WIMP and mediator  $a$ .  $m_A$  is the mass eigenvalue of the mediator  $A$ .  $m_h$ ,  $m_H$ ,  $m_{H^\pm}$  and  $m_{H^-}$  are the mass eigenvalues of the higgs sectors  $h$ ,  $H$ ,  $H^+$  and  $H^-$ , respectively. Under this assumption, the normalized exclusion limit dependence (95% C.L.) on the WIMP mass is calculated and shown in Fig. 6. The normalized limit is expressed in terms of the ratio of the excluded cross section ( $\sigma$ ) to the nominal cross section of the model ( $\sigma_{\text{theory}}$ ). The nominal cross section is determined under the assumption that the couplings satisfy  $g_q = g_\chi = 1$ , as the Ref. [34] shows. Compared to the exclusion area set by ATLAS [34], PandaX-4T experiment is more sensitive when  $m_\chi$  is above several hundred  $\text{GeV}/c^2$ .

In conclusion, this letter presents the new limits on WIMP-nucleus SD interaction cross section from PandaX-4T commissioning data. The data analysis method, background models and statistical inference are identical to the PandaX-4T SI analysis [5]. The most stringent upper limit (90% C.L.) on WIMP-neutron cross section in direct search experiment is obtained, with the lowest value of  $5.8 \times 10^{-42} \text{ cm}^2$  at WIMP mass of 40  $\text{GeV}/c^2$ . The WIMP-proton interaction cross section

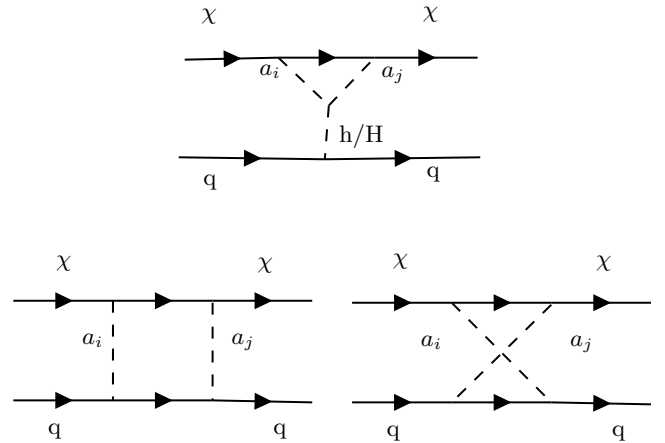


FIG. 5. The upper panel is the triangle diagram of scattering between dark matter in 2HDM+a model and nuclei [33].  $a_i, a_j$  represents the mediator  $a/A$ . The lower panel is the corresponding box diagrams in 2HDM+a model [33].  $a_i, a_j$  represents the mediator  $a/A$ .

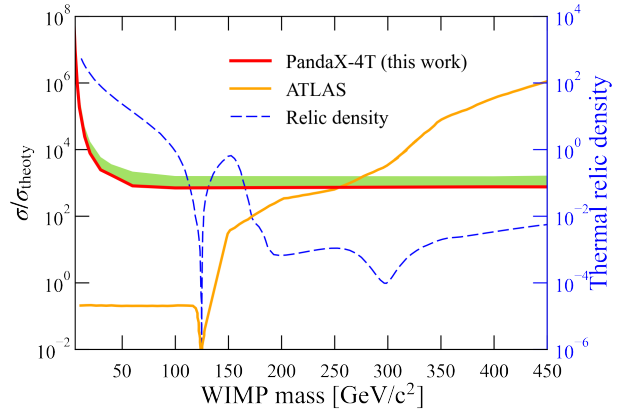


FIG. 6. PandaX-4T 95% C.L. normalized exclusion limit (red solid) for pseudo-scalar mediator model as a function of WIMP mass. The green band shows the  $\pm 1\sigma$  sensitivity band. The normalized limit is expressed in terms of the ratio of the excluded cross section to the nominal cross section of the model. The 95% C.L. from ATLAS [34] (orange solid) is also shown for comparison. The relic density (blue dashed) for each WIMP mass [34] is overlaid and described by the right blue axis, based on the parameters shown in (5).

constraint at 90% C.L. is also obtained with the lowest value of  $1.7 \times 10^{-40} \text{ cm}^2$  at WIMP mass of 40  $\text{GeV}/c^2$ . In addition, the exclusion limits (95% C.L.) for two distinct simplified models are also calculated. Both the tree-level contribution and the loop-level contribution are considered. This result is complementary to that obtained from the collider experiment (ATLAS [27, 34] and CMS [28]) in the WIMP mass region above several hundred  $\text{GeV}/c^2$ . The PandaX-4T experiment continues taking physics data and will scan unexplored parameter space further.

We would like to thank Tong Li and Wei Chao for helpful discussion. This project is supported in part by grants from National Science Foundation of China (Nos. 1209061, 12005131, 11905128, 11925502, 11735003, 11775141), a grant from the Ministry of Science and Technology of China (No. 2016YFA0400301), and by Office of Science and Technology, Shanghai Municipal Government (grant No. 18JC1410200). We thank supports from Double First Class Plan of the Shanghai Jiao Tong University. We also thank the sponsorship from the Chinese Academy of Sciences Center for Excellence in Particle Physics (CCEPP), Hongwen Foundation in Hong Kong, Tencent Foundation in China and Yangyang Development Fund. Finally, we thank the CJPL administration and the Yalong River Hydropower Development Company Ltd. for indispensable logistical support and other help.

---

\* Spokesperson: jianglai.liu@sjtu.edu.cn

† Corresponding author: nzhou@sjtu.edu.cn

- [1] Gianfranco Bertone, Dan Hooper, and Joseph Silk. Particle dark matter: Evidence, candidates and constraints. *Phys. Rept.*, 405:279–390, 2005.
- [2] D. S. Akerib et al. Results from a search for dark matter in the complete LUX exposure. *Phys. Rev. Lett.*, 118(2):021303, 2017.
- [3] Xiang Xiao et al. Low-mass dark matter search results from full exposure of the PandaX-I experiment. *Phys. Rev. D*, 92(5):052004, 2015.
- [4] Qihong Wang et al. Results of dark matter search using the full PandaX-II exposure. *Chin. Phys. C*, 44(12):125001, 2020.
- [5] Yue Meng et al. Dark Matter Search Results from the PandaX-4T Commissioning Run. *Phys. Rev. Lett.*, 127(26):261802, 2021.
- [6] E. Aprile et al. XENON100 Dark Matter Results from a Combination of 477 Live Days. *Phys. Rev. D*, 94(12):122001, 2016.
- [7] E. Aprile et al. Dark Matter Search Results from a One Ton-Year Exposure of XENON1T. *Phys. Rev. Lett.*, 121(11):111302, 2018.
- [8] Yu-Cheng Wu et al. Measurement of Cosmic Ray Flux in China JinPing underground Laboratory. *Chin. Phys. C*, 37(8):086001, 2013.
- [9] Zhao-Ming Zeng, Hui Gong, Jian-Min Li, Qian Yue, Zhi Zeng, and Jian-Ping Cheng. Design of the thermal neutron detection system for CJPL-II. *Chin. Phys. C*, 41(5):056002, 2017.
- [10] Hongguang Zhang et al. Dark matter direct search sensitivity of the PandaX-4T experiment. *Sci. China Phys. Mech. Astron.*, 62(3):31011, 2019.
- [11] Zhou Huang et al. Neutron-induced nuclear recoil background in the pandax-4t experiment. *Chinese Physics C*, 2022.
- [12] Nicole F. Bell, Giorgio Busoni, and Isaac W. Sanderson. Loop Effects in Direct Detection. *JCAP*, 08:017, 2018. [Erratum: *JCAP* 01, E01 (2019)].
- [13] T. Alanne, F. Bishara, J. Fiaschi, O. Fischer, M. Gorbahn, and U. Moldanazarova.  $Z'$ -mediated Majorana dark matter: suppressed direct-detection rate and complementarity of LHC searches. 2 2022.
- [14] Jingkai Xia et al. PandaX-II Constraints on Spin-Dependent WIMP-Nucleon Effective Interactions. *Phys. Lett. B*, 792:193–198, 2019.
- [15] E. Aprile et al. Constraining the spin-dependent WIMP-nucleon cross sections with XENON1T. *Phys. Rev. Lett.*, 122(14):141301, 2019.
- [16] P. Klos, J. Menéndez, D. Gazit, and A. Schwenk. Large-scale nuclear structure calculations for spin-dependent WIMP scattering with chiral effective field theory currents. *Phys. Rev. D*, 88(8):083516, 2013. [Erratum: *Phys.Rev.D* 89, 029901 (2014)].
- [17] Fady Bishara, Joachim Brod, Benjamin Grinstein, and Jure Zupan. From quarks to nucleons in dark matter direct detection. *JHEP*, 11:059, 2017.
- [18] Fady Bishara, Joachim Brod, Benjamin Grinstein, and Jure Zupan. DirectDM: a tool for dark matter direct detection. 8 2017.
- [19] C. Savage, G. Gelmini, P. Gondolo, and K. Freese. Compatibility of DAMA/LIBRA dark matter detection with other searches. *JCAP*, 04:010, 2009.
- [20] J. D. Lewin and P. F. Smith. Review of mathematics, numerical factors, and corrections for dark matter experiments based on elastic nuclear recoil. *Astropart. Phys.*, 6:87–112, 1996.
- [21] D. Baxter et al. Recommended conventions for reporting results from direct dark matter searches. *Eur. Phys. J. C*, 81(10):907, 2021.
- [22] C. Amole et al. Dark Matter Search Results from the Complete Exposure of the PICO-60 C<sub>3</sub>F<sub>8</sub> Bubble Chamber. *Phys. Rev. D*, 100(2):022001, 2019.
- [23] Tomohiro Abe et al. LHC Dark Matter Working Group: Next-generation spin-0 dark matter models. *Phys. Dark Univ.*, 27:100351, 2020.
- [24] Antonio Boveia et al. Recommendations on presenting LHC searches for missing transverse energy signals using simplified  $s$ -channel models of dark matter. *Phys. Dark Univ.*, 27:100365, 2020.
- [25] Matthew R. Buckley, David Feld, and Dorival Goncalves. Scalar Simplified Models for Dark Matter. *Phys. Rev. D*, 91:015017, 2015.
- [26] Wei Chao. Direct detections of Majorana dark matter in vector portal. *JHEP*, 11:013, 2019.
- [27] Georges Aad et al. Search for new phenomena in events with an energetic jet and missing transverse momentum in  $pp$  collisions at  $\sqrt{s} = 13$  TeV with the ATLAS detector. *Phys. Rev. D*, 103(11):112006, 2021.
- [28] Armen Tumasyan et al. Search for new particles in events with energetic jets and large missing transverse momentum in proton-proton collisions at  $\sqrt{s} = 13$  TeV. *JHEP*, 11:153, 2021.
- [29] C. Amole et al. Dark Matter Search Results from the PICO-60 C<sub>3</sub>F<sub>8</sub> Bubble Chamber. *Phys. Rev. Lett.*, 118(25):251301, 2017.
- [30] Francesco D’Eramo, Bradley J. Kavanagh, and Paolo Panci. You can hide but you have to run: direct detection with vector mediators. *JHEP*, 08:111, 2016.
- [31] Tong Li. Revisiting the direct detection of dark matter in simplified models. *Phys. Lett. B*, 782:497–502, 2018.
- [32] Tong Li and Peiwen Wu. Simplified dark matter models with loop effects in direct detection and the constraints from indirect detection and collider search. *Chin. Phys.*

- C*, 43(11):113102, 2019.
- [33] Tomohiro Abe, Motoko Fujiwara, and Junji Hisano. Loop corrections to dark matter direct detection in a pseudoscalar mediator dark matter model. *JHEP*, 2019(2):28, February 2019.
- [34] Morad Aaboud et al. Constraints on mediator-based dark matter and scalar dark energy models using  $\sqrt{s} = 13$  TeV  $pp$  collision data collected by the ATLAS detector. *JHEP*, 05:142, 2019.